FISEVIER

Contents lists available at ScienceDirect

## Applied Surface Science

journal homepage: www.elsevier.com/locate/apsusc



### Full Length Article

# Assessing microbially influenced corrosion of titanium as novel canister material for geological disposal facilities

Adam D. Mumford <sup>a</sup>, Marcos F. Martinez-Moreno <sup>b,e</sup>, Mar Morales-Hidalgo <sup>b</sup>, Cristina Povedano-Priego <sup>b</sup>, Lidia Generelo-Casajus <sup>b</sup>, Fadwa Jroundi <sup>b</sup>, Lorna Anguilano <sup>c</sup>, Uchechukwu Onwukwe <sup>c</sup>, Philip H.E. Gardiner <sup>d</sup>, Mohamed L. Merroun <sup>b</sup>, Yon Ju-Nam <sup>a</sup>, Jesus J. Ojeda <sup>a,\*</sup>

- a Department of Chemical Engineering, Faculty of Science and Engineering, Swansea University, Swansea, United Kingdom
- <sup>b</sup> Faculty of Sciences, Department of Microbiology, University of Granada, Granada, Spain
- c Experimental Techniques Centre, Brunel University London, Uxbridge, United Kingdom
- <sup>d</sup> Biomolecular Sciences Research Centre, Sheffield Hallam University, Sheffield, United Kingdom
- <sup>e</sup> Current address: Institute of Resource Ecology, Helmholtz-Zentrum Dresden-Rossendorf, Dresden, Germany

#### ARTICLE INFO

# Keywords: Corrosion Titanium Nuclear waste Geological Disposal Facilities (GDFs) Microbially Influenced Corrosion (MIC)

#### ABSTRACT

In response to the growing global inventory of nuclear waste and the urgent need for secure long-term disposal solutions, geological disposal facilities (GDFs), also known as deep geological repositories, are being pursued worldwide. Several national programmes, including those in the UK, Japan, and Canada, are evaluating corrosion-resistant alloys for waste canisters. Among these, novel materials such as titanium alloys have emerged as promising candidates due to their protective TiO<sub>2</sub> films. However, the threat of microbial corrosion under repository-relevant conditions remains highly unexplored. To address this, titanium discs (grade 2, ASTM B348) were incubated in bentonite slurries with synthetic pore-water at 30 °C and 60 °C under strictly anoxic, dark conditions, mimicking deep underground GDF environments. Electron donors (acetate, lactate) and an electron acceptor (sulphate) were added to stimulate microbial activity and assess long-term canister performance. All titanium samples retained an intact TiO<sub>2</sub> layer with no detectable pitting or localised damage. Microscopic (SEM) and spectroscopic (XPS) analyses showed slight thinning of titanium oxide films and microbial presence colocated with bentonite, but no evidence of corrosion products or metal loss. Micro-FTIR showed functional groups associated with microbial presence (proteins, lipids, and polysaccharides) in the bentonite, but not on titanium surfaces. The experimental design aimed to promote bacterial activity by simulating worst-case GDF biotic conditions.

These findings demonstrate titanium's exceptional stability against microbially influenced corrosion (MIC) in stimulated GDF-like environments. This study supports the structural viability of titanium canisters for nuclear waste disposal and underscores the importance of considering microbial factors in long-term corrosion assessments.

#### 1. Introduction

As countries increasingly turn to nuclear power for energy security and climate change mitigation, the issue of managing the resultant high-level waste (HLW) continues to be a major challenge. Despite representing <1% of the total waste volume, HLW contains 98% of the total radioactivity [1]. These waste products emit considerable heat as a result of the radioactive decay process and contain substantial amounts

of long-lived radionuclides, which have half-lives up to millions of years [2,3]. As of recent estimates, approximately 22,000 m<sup>3</sup> of HLW is stored worldwide, and none of it has been permanently disposed [4]. Safe, long-term storage of nuclear waste is a global goal, with geological disposal facilities (GDFs), also known as deep geological repositories (DGRs), being deemed as the best solution for the final storage of HLW [5]. GDFs incorporate engineered and natural barriers, each serving specific functions to provide successive layers of protection against the

E-mail address: j.j.ojedaledo@swansea.ac.uk (J.J. Ojeda).

<sup>\*</sup> Corresponding author.

potential release of radioactive materials into the environment. Typically, these protective layers consist of a combination of natural geological formations (host rock) and engineered components with metal canisters at the core, which is surrounded by clay buffers and backfill materials (typically bentonite).

Abiotic corrosion resistance of metals under GDF-relevant conditions is generally well documented. However, microbially induced corrosion (MIC) under these conditions is far less known. Despite the early assumption that the highly radioactive nature of HLW would make bacterial activity challenging in these areas, microorganisms are remarkably adaptable and can thrive in the challenging environments within GDFs [6–9]. Notably, indigenous microorganisms, including sulphate reducing bacteria (SRB), have been isolated from bentonite materials [10–14]. Corrosion by SRB is particularly aggressive and localised. Therefore, they are responsible for approximately 50 % of all cases of MIC [15]. Microorganisms can persist in GDFs by surviving in a nearly inactive metabolic state or as spores, even for long periods of time [16,17]. This underscores that GDFs cannot be considered sterile environments, as microbes have been shown to withstand these extreme conditions.

The canister material and design are crucial for ensuring the long-term containment of nuclear waste, preventing radionuclide migration, and safeguarding human health and the environment. Copper is favoured in Sweden and Finland for canister design, whilst the carbon steel option is still being explored predominantly in France and Switzerland [18–20]. Countries such as the UK, Japan, and Canada have either considered or are considering titanium as a potential material for nuclear waste canisters, mainly due to its outstanding corrosion resistance and ability to form stable, protective oxide films that enhance durability [21–23]. The suitability of this metal is further supported by its compatibility with bentonite, the most common backfill/buffer material, making it a promising option for long-term waste containment.

However, despite the titanium corrosion resistance, the influence of microbiological and physico-chemical parameters—such as microbial activity, sulphide generation, and temperature—on its long-term corrosion behaviour under GDF-relevant conditions remains largely unexplored [10,21,24,25]. Assessing the interactions between titanium surfaces and both indigenous and introduced microbial communities, particularly under anoxic and bentonite-saturated conditions, is essential for evaluating its suitability as a waste canister material. This study investigates titanium resistance to MIC, with specific consideration of SRB activity, under biotically stimulated GDF-relevant conditions, replicated in purposely designed microcosms. A multi-technique approach was applied to evaluate changes in surface chemistry and corrosion behaviour after exposure, providing a detailed assessment of titanium MIC resistance in these environments.

#### 2. Materials and methods

#### 2.1. Titanium discs

Grade 2 (ASTM B348) titanium rods (99.6 % purity) were purchased at a diameter and length of 16 mm and 20 cm, respectively, and then cut into 4 mm thick discs. These titanium discs were treated following an established protocol [26], to remove any grease, debris, or biological matter from the surface and to 'reset' the passive oxide layer after the cutting process. This was primarily done to reduce the variation of oxides, as  $\text{TiO}_2$  is known to dictate the corrosion behaviour of titanium [1,2]. This process consisted of three separate sonication treatments in the following order: technical grade ethanol, UHQ water, and nitric acid (10 mM), followed by an UHQ water rinse. This procedure was repeated three times for each disc.

#### 2.2. Bentonite collection

Bentonite samples were collected from the clay formation at "El Cortijo de Archidona" in Almeria, Spain, in January 2020. This bentonite is a calcium-magnesium-sodium montmorillonite originating from the alteration of pyroclastic volcanic rocks. During the bentonite sampling and processing, contamination was mitigated by using sterilised containers. Subsequently, the samples were allowed to dry inside a laminar flow chamber for 5 days and then stored at 4  $^{\circ}\mathrm{C}$  until manually ground. Finally, the bentonite samples were further ground into a roughly homogeneous powder, using a stainless-steel roller under aseptic conditions.

#### 2.3. Experimental set-up

Microcosms designed to simulate biotically stimulated GDF-relevant conditions were assembled following the protocol outlined in Povedano-Priego et al. (see Fig. 1) [27]. Twenty-four sterile borosilicate-glass bottles (250 mL), with butyl-rubber stoppers, were used. Each bottle contained 35 g of ground bentonite saturated with 170 mL of synthetic pore-water prepared following a method from Fernandez et al. [28,29] (see Supplementary Information S1). Anoxic conditions were established by sealing the microcosms with butyl rubber stoppers and purging them with  $\rm N_2$  gas for 20 min, displacing the oxygen inside the microcosms. All microcosms were kept anoxic, and sampling was undertaken in an anaerobic chamber.

Some microcosms were inoculated with either an aerobic or anaerobic bacterial consortium denoted as BaC and BanC, respectively. Each consortium was composed of multiple bacterial genera previously identified in FEBEX bentonite, see Table 1 [12,16,30–33].

For the aerobic consortium, *Amycolatopsis ruanii* was incubated in yeast-malt-glucose (YMG) medium, while all others were incubated in lysogenic broth (LB). The anaerobic consortium consisted of four types of SRB which are among the most commonly cited bacterial culprits of MIC [34–36]. These were incubated in their respective culture media under anoxic conditions, with media preparation conducted according to the manufacturer's guidelines (see Supplementary information S2) [37]. For samples without bacterial consortia, only filtered culture media were added. This was done to increase the comparability and reduce the variation between samples with and without added consortia. Lastly, 'blank' samples at each temperature were made by using 170 ml of artificial pore-water and a titanium disc sample.

To replicate the conditions of a GDF, microcosms were incubated under anoxic conditions, at temperatures of 30 or 60 °C, and in complete darkness. These temperatures were selected to represent repositoryrelevant conditions: 30 °C approximates ambient subsurface temperatures, while 60 °C reflects the peak near-field values predicted during the early thermal-saturation transient, where radiogenic heating may raise bentonite buffer temperatures to 60–90 °C before cooling over time [38-41]. To accelerate MIC processes, electron donors (30 mM sodium acetate and 10 mM sodium lactate) and an electron acceptor (20 mM sodium sulphate) were added [27,30,42]. This amendment aimed to enhance microbial activity and accelerate any potential corrosion by creating a worst-case biotic scenario, allowing for the evaluation of metal performance over extended periods within the constraints of a practical experimental timeline. Previous studies with this bentonite have shown that tyndallisation (autoclaving at 110 °C, 45 min, 3 consecutive days) did not completely eliminate microbial activity in the bentonite, only reduced it, due to two main reasons: (1) the physicochemical properties of bentonite (e.g., low permeability or thermal conductivity) and (2) the presence of high-temperature resistant spore-forming bacteria, including some sulphate-reducing bacteria viable even under these treatments [16,42-44]. In addition, previously reported data [37] demonstrated that the microorganisms present in the bentonite can

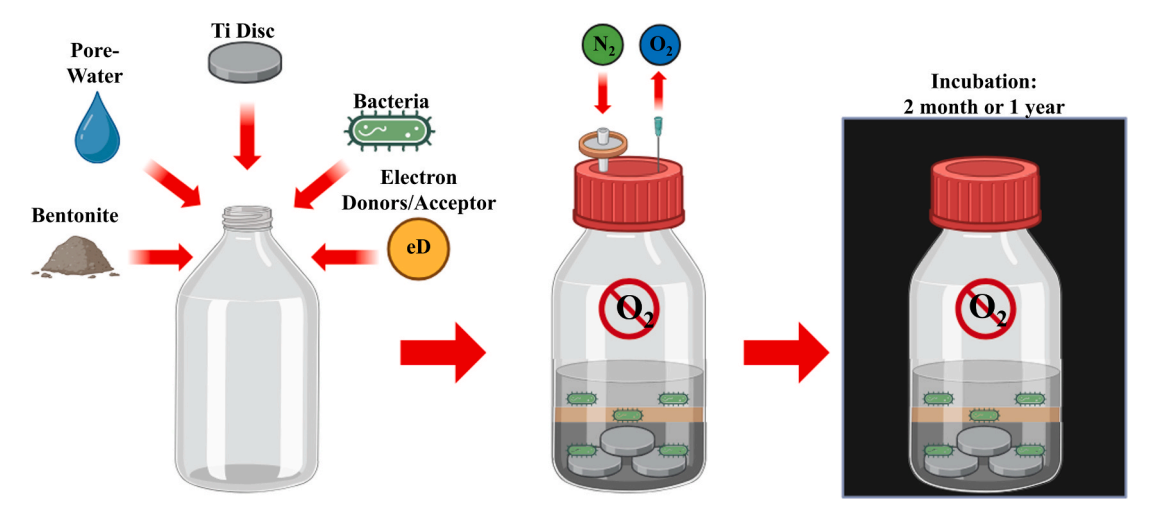


Fig. 1. Microcosm creation workflow depicting the addition of various components, the nitrogen gas purge, and the dark incubation of the microcosms for 2 months and 1 year (created with Biorender.com).

Table 1
Aerobic and anaerobic bacterial consortia used in the different microcosms.

Aerobic bacterial consortium (aC)	Anaerobic bacterial consortium (anC)
Stenotrophomonas bentonitica (BII-R7) Bacillus sp. (BII-C3) Pseudomonas putida, ATCC33015 <sup>a</sup> Amycolatopsis ruanii, NCIMB14711 <sup>b</sup>	Desulfuromonas sp., DSM 101009° Desulfosporosinus acidiphilus, DSM 22704° Desulfovibrio desulfuricans, DSM 642° Desulfotomaculum reducens, DSM 100969° Geobacter metallireducens, DSM 710°

- <sup>a</sup> American type culture collection.
- <sup>b</sup> National collection of industrial food and marine bacteria.
- <sup>c</sup> Leibniz Institute DSMZ.

withstand harsh conditions such as elevated temperatures and gamma irradiation. For these reasons, controls with sterile bentonite are not realistic since traditional sterilisation methods (e.g., autoclaving by tyndallisation) do not ensure the complete sterilisation of the bentonite. In total, 10 treatments were considered and prepared in triplicate, obtaining a total of 30 microcosms. Each treatment is shown and detailed in Table 2.

#### 2.4. X-ray photoelectron spectroscopy

The surfaces of the titanium discs were analysed using a Kratos AXIS Supra Photoelectron Spectrometer. The unit employed a monochromated Al K $\alpha$  X-ray source (1486.6 eV), configured to 20 mA X-ray emission current and a 15 kV acceleration voltage (anode high tension). The sample plane was aligned to a fixed take-off angle of 90°. Data acquisition was carried out at three randomly selected sites, with each

measurement covering a rectangular area of approximately 110  $\mu m \times 110~\mu m$  using the FOV2 lens. Analysis included a wide survey scan at 160 eV pass energy with 1.0 eV steps and a high-resolution scan at 20 eV pass energy with 0.1 eV steps for detailed component analysis. Differential charging was mitigated using the integrated Kratos charge neutraliser. Binding energies were calibrated based on Au 4f5/2 (83.9 eV), and Ag 3d5/2 (368.27 eV), Cu 2p3/2 (932.7 eV) lines of cleaned copper, gold, and silver standards from the National Physical Laboratory (NPL), UK. CasaXPS 2.3.22 [45] software was used to fit the XPS spectra peaks. All binding energies were referenced to the C1s adventitious carbon peak at 285 eV to correct any potential surface charging effects. No further constraints were imposed on the initial binding energy values. No sample preparation was performed, to preserve any potential corrosion products adhered to the surface of the discs.

#### 2.5. Micro-Fourier transform infrared spectroscopy

Reflectance micro-Fourier Transform Infrared Spectroscopy (micro-FTIR) was used to analyse the titanium discs and assess the presence of biological material. No sample preparation was performed to preserve any potential corrosion products or biofilm formation after incubation. Reflectance micro-FTIR images were obtained using a PerkinElmer Spotlight micro-FTIR spectroscope, equipped with a mercury–cadmium–telluride detector (consisting of 16 gold-wired infrared detector elements). A per-pixel aperture size of 25  $\mu m \times 25 \ \mu m$  was used with two co-added scans per pixel and a spectral resolution of 16 cm $^{-1}$ .

Table 2
Treatments of each microcosm including their respective tag. Treatment conditions: Bentonite, Electron Donors/Acceptor, Aerobic Consortium, Anaerobic Consortium, and Incubation temperatures. All samples contained Pore-water and were all incubated for both 2 months and 1 year. B = Bentonite, aC = aerobic bacterial consortia, anC = anaerobic bacterial consortia.

Sample name	Bentonite	Electron donors/acceptor	Aerobic consortium (aC)	Anaerobic consortium (anC)	30 °C	60 °C
30 B	+	+	_	_	+	_
30 BaC	+	+	+	_	+	_
30 BanC	+	+	_	+	+	_
60 B	+	+	_	_	_	+
60 BaC	+	+	+	_	_	+
60 BanC	+	+	_	+	_	+
30 B (Blank)	+	_	_	_	+	_
60 B (Blank)	+	_	_	_	_	+
30 Blank	_	_	_	_	+	_
60 Blank	_	_	_	_	_	+

#### 2.6. Scanning electron microscopy

Samples were analysed using a Tescan Magna STEM, fitted with an Oxford energy dispersive X-ray spectrometer for elemental microanalysis. Prior to analysis, the samples were sputtered with a thin layer of electron-transparent carbon coating to improve conductivity under the electron beam. No further pre-treatment was used to maintain the integrity of any potential corrosion products on the surface of the discs.

#### 2.7. Inductively coupled plasma mass spectrometry

The concentration of both sulphur and the potential dissolved metals in the pore-water of the incubated samples was quantified using a PerkinElmer NexION 350X Inductively Coupled Plasma Mass Spectrometer (ICP-MS). Under anaerobic conditions, the supernatants were sampled and filtered using a 0.22  $\mu m$ -sterile filter. Samples were diluted using nitric acid to redissolve any potential precipitates in the liquid. Calibration was carried out by using multi-element calibration solutions containing Al, Ti, Fe, S, and Si, and indium as internal standard.

#### 3. Results and discussion

#### 3.1. Visual changes

During the incubation period, visual colour changes occurred in all microcosms. Fig. 2 shows one representative microcosm from each triplicate and illustrates the colour changes in the bentonite and supernatant over three time periods: time zero (t = 0), two months (t = 0) 2m), and one year (t = 1y). At 30  $^{\circ}$ C, all samples equally exhibited the most drastic colour change. From t=0 to t=2m, clear differences could be observed: the bentonite changed from a cream, sand-like colour to black, and the pore-water from clear to black (Fig. 2). This change was more pronounced after one year of incubation (t = 1y) as the pore-water appeared to slightly darken further. In comparison, the samples incubated at 60 °C, specifically 60B and 60BanC, showed few changes to their colour. The only evident change was the darkening of the porewater in these samples. However, the ones inoculated with aerobic bacteria showed similar results to the 30 °C incubated microcosms. It is important to note that, although samples 30B and 60B did not have additional bacterial consortia, they are not necessarily abiotic as the native bacterial communities were not disturbed by any sterilisation process. Furthermore, studies have previously indicated the growth of bentonite-indigenous SRB microbial populations and consequently, biotic factors could also be responsible for the colour changes [27,30,44].

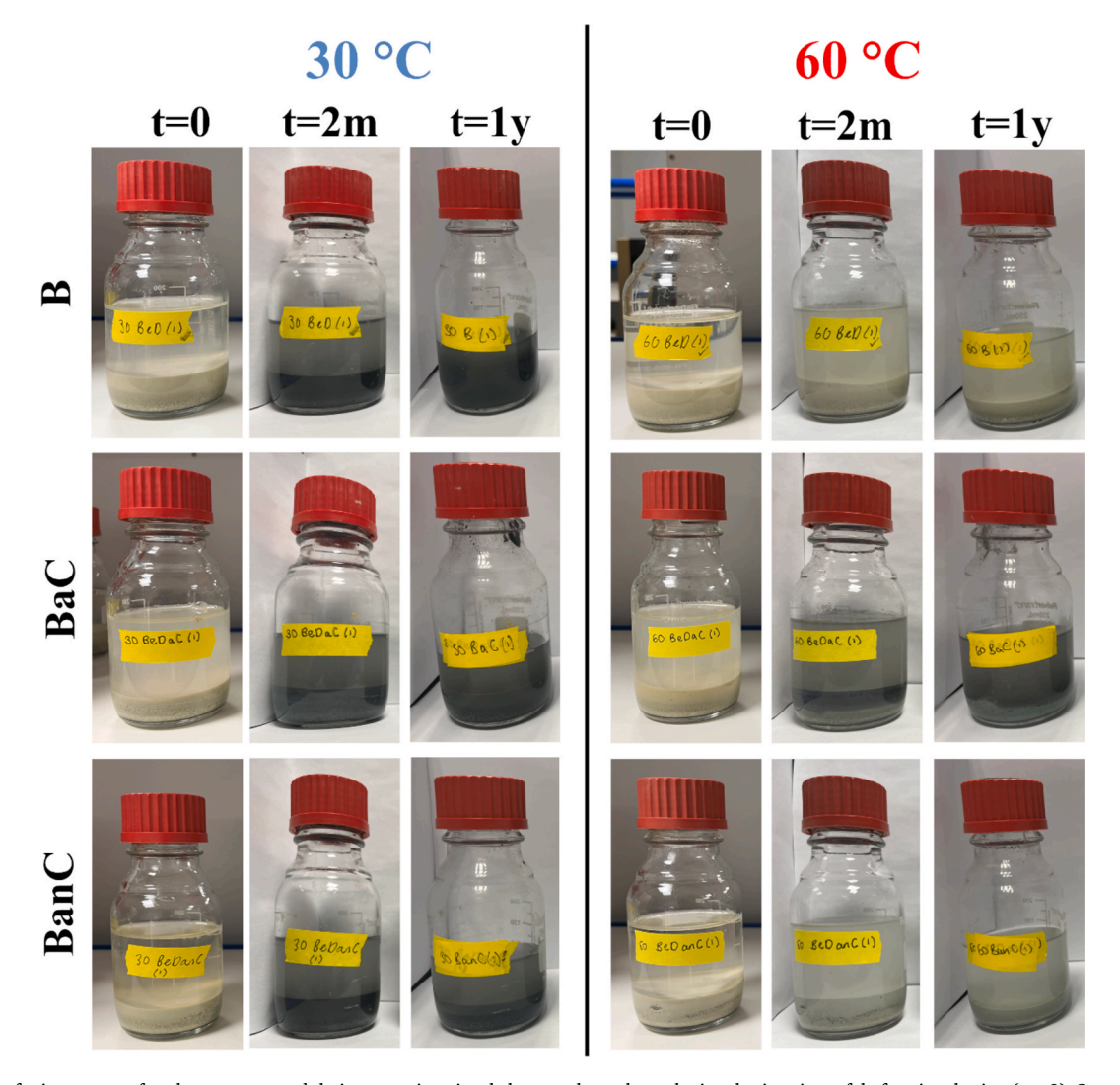


Fig. 2. Photos of microcosms of each treatment and their respective visual changes throughout the incubation time of; before incubation (t = 0), 2 months incubation (t = 2m), and 1 year incubation (t = 1y).

Previous studies have attributed the darkening of bentonite to interactions between  $\rm H_2S$  produced by bacteria and the metals inside the bentonite, such as iron [46,47]. The reaction of  $\rm H_2S$  and Fe can produce FeS, which is of dark grey/black colour. FeS could also dissipate into the surrounding solution (pore-water), potentially forming black precipitates [46,47].

The darkening of bentonite and pore-water was evident in all microcosms incubated at 30 °C. However, at 60 °C, only the microcosms inoculated with the aerobic bacterial consortium (aC) showed comparable levels of darkening. The less-intense colour changes at 60 °C in the microcosms 60BanC and 60B could be explained by the optimum growth temperatures of the bacteria in both the anaerobic consortia and the bentonite-indigenous bacteria. The microbial population in these samples contained genera with optimum growth temperatures at a maximum of 37 °C (except for Desulfotomaculum), meaning any rise in temperature above this may generally decrease bacterial productivity. This is consistent with previous studies that reported inhibition of SRB at 60 °C in bentonite systems [43,46]. While the observed colour change could be attributed to bacterial activity [48,49], some abiotic reasons may also play a role. These include mineral precipitation from the bentonite into the pore-water, such as the formation of magnetite  $(Fe_3O_4)$ , or the oxidation of  $Fe^{2+}$  to  $Fe^{3+}$ , leading to the development of dark oxides/hydroxides [50]. In the case of 60BaC, the blackening does not necessarily reflect sustained SRB activity but may result from transient sulphide production early in incubation, which even at trace levels can react with Fe<sup>2+</sup> to form FeS [51]. Facultative thermotolerant genera such as Pseudomonas, which has been found to dominate bentonite microbial community at 60 °C of incubation [43], may also contribute to the reduction of Fe(III) [52], and increasing Fe<sup>2+</sup> availability for FeS precipitation. Furthermore, genera such as Clostridium have been identified in this bentonite and has the propensity to reduce sulphates to sulphur, despite the high temperature [27,53,54]. Additional non-SRB sulphur cycling pathways, such as thiosulphate or elemental sulphur reduction, may further generate reduced sulphur species under these conditions [55,56]. No colour change was observed in the microcosms 60B (Blank) (natural bentonite, no added consortia, no added electron donors), whilst 30B (Blank) did show darkening of the bentonite (see supplementary information S3). This further supports the suggestion that temperature is a variable affecting the colour change, potentially by limiting the bentonite-indigenous bacteria growth and hence the biotic generation of FeS compounds.

#### 3.2. XPS

After two months (t=2m) and one year (t=1y) of incubation, discs were collected from the microcosms. These were then analysed using XPS to investigate the effect of each treatment on the surface chemistry of the discs. Wide scans showed the presence of Mg, Na, O, Ti, Ca, C, Cl, S, P, Si and Al, with Mg, Cl, S, P and Al not being found prior to incubation on the clean titanium discs (t=0). Chlorine and sulphur were present in the artificial pore-water, and aluminium is commonly found in bentonite. The wide XPS spectra of all titanium discs are shown in Supplementary Information S4.

High-resolution titanium (Ti 2p) region scans, between 474 and 449 eV, were acquired to understand the variation of titanium oxidation states (Supplementary Information S5, Figs. 3 and 4). The Ti 2p spectra were deconvoluted and fitted in order to evaluate and quantify the distribution of oxidation states on the surface of the discs (see Supplementary Information S5). The resulting fitting values were as follows: the intensity ratio of Ti  $2p_{3/2}$  and Ti  $2p_{1/2}$  was 2:1, and the FWHM at 1.04 for Ti(IV)  $2p_{3/2}$ , Ti(III) at 1.4, 1.6 for Ti(II), and 0.69 for Ti(0)  $2p_{3/2}$ , all of which correspond to literature [57–59]. In all samples, Ti(0),  $2p_{3/2}$  peak was observed around 453.9 eV. To deconvolute the corresponding Ti  $2p_{1/2}$  peak, a spin–orbit splitting of 6.1 eV between the  $2p_{3/2}$  and  $2p_{1/2}$  peaks was used, as found in the literature [57,58,60]. The peak observed around 455.5 eV has been previously assigned to Ti (II) oxide

 $2p_{3/2}$ , with a splitting of 5.6 eV for its corresponding  $2p_{1/2}$  signal [57,58,61]. Ti(III),  $2p_{3/2}$ , oxide was observed at 457.3 eV, with a splitting of 5.2 eV [61]. Finally, Ti(IV) oxide (TiO<sub>2</sub>),  $2p_{3/2}$ , was found at around 458.7 eV, with a splitting of 5.7 eV [57,58,60,61].

The resulting deconvoluted spectra for samples incubated at 30 °C (Fig. 3) and 60 °C (Fig. 6) allowed for the quantification of oxidation states on the scanned surface of the titanium discs by atomic percentage (At%), and were compared to the clean titanium disc at t=0 (Blank, Supplementary Information S5). Higher amounts of Ti(0) were observed on all treated samples at 30 and 60 °C when compared to the blank, indicating the thinning or disruption of the  $\text{TiO}_{x}$  protective layer and potentially exposing the unprotected metal layer to localised corrosion. However, it should be noted that although there was an observed reduction in the  $\text{TiO}_{2}$  contribution on all samples post-treatment, the At % was never below 70 %, indicating that the surface of the discs was still predominantly made of  $\text{TiO}_{2}$ .

When comparing the discs surfaces incubated at 30 °C between 2 months and 1 year incubation (Fig. 5), an increase in the At% of Ti metal signal was seen on the surface of sample BaC, potentially demonstrating the thinning of the TiO $_2$  layer. This is further supported by the fact that the sample also showed an  $\sim\!11$ % decrease in At% of TiO $_2$  on the surface over this time period. Conversely, sample 30B, from 2 months to 1 year demonstrated an overall decrease in At% of Ti metal whilst showing little change in the At% of TiO $_2$ — suggesting minimal disruption of the protective passive layer. Similarly, sample 30BanC showed no signs of oxide layer deterioration between 2 months and 1 year of incubation. However, it exhibited a notably high atomic percentage (At%) of Ti metal after 2 months — the highest At% observed amongst samples incubated at 30 °C.

Sample 60B showed an increase in Ti metal At%, whilst exhibiting a  $\sim$ 10 % decrease in TiO<sub>2</sub>, potentially indicating the thinning of the oxide layer (Fig. 4). On the other hand, sample 60BaC showed a small decrease in the At% of both Ti metal and TiO2 on the surface. Adding this to the increase in the At% of Ti<sub>2</sub>O<sub>3</sub> observed, this suggested a decrease in proportion of TiO<sub>2</sub> in the protective oxide layer, potentially reducing its stability. Sample 60BanC did not exhibit much difference in the At% of TiO<sub>2</sub> or Ti metal but did show a decrease in the At% of TiO, falling below the limit of detection. All samples incubated at 60 °C showed Ti metal At % equal to or greater than those of their counterparts incubated at 30 °C, suggesting that temperature plays a role in influencing the stability, thickness, and coverage of the passive layer. Further comparison shows that the samples incubated at 60 °C with added anaerobic consortia, presented the highest values of At% across all incubation times. This, alongside the increase in Ti(0) signal for sample 30 BanC, could suggest that the added anaerobic consortia can potentially contribute to the slight thinning or disruption of the protective oxide layer. However, the observed changes in Ti metal and oxide signals are attributed to variations in oxide thickness, rather than to sulphide formation, as supported by the S 2p spectra (supplementary information S6).

Titanium's passive oxide layer typically consists of TiO,  $Ti_2O_3$ , and  $TiO_2$ , with  $TiO_2$  being the most stable and protective against corrosion, while the less stable TiO and  $Ti_2O_3$  are formed under oxygen-deficient conditions and offer limited passivity [62,63]. The predominance of  $TiO_2$  in the passive oxide layer is critical for titanium's corrosion resistance, particularly in environments containing SRB at elevated temperatures [63].  $TiO_2$  is the most thermodynamically stable oxide, with a Gibbs free energy of formation ( $\Delta Gf^{\circ}$ ) of -889 kJ/mol, compared to TiO(-516 kJ/mol) and  $Ti_2O_3$  (-765 kJ/mol), providing superior chemical stability and resistance to dissolution [25,64,65]. The presence of Ti(O) indicates thinning or disruption of the oxide, exposing the substrate to localised corrosion, governed by:

$$Ti + 2H_2O \rightarrow TiO_2 + 4H^+ + 4e^-$$
 (1)

TiO<sub>2</sub> also exhibits low electronic conductivity ( $\sim 10^{-12}~\Omega~cm^{-1}$ ) minimising electrochemical reactions. Its self-healing nature ensures rapid regeneration of the protective film, while its crystalline forms,

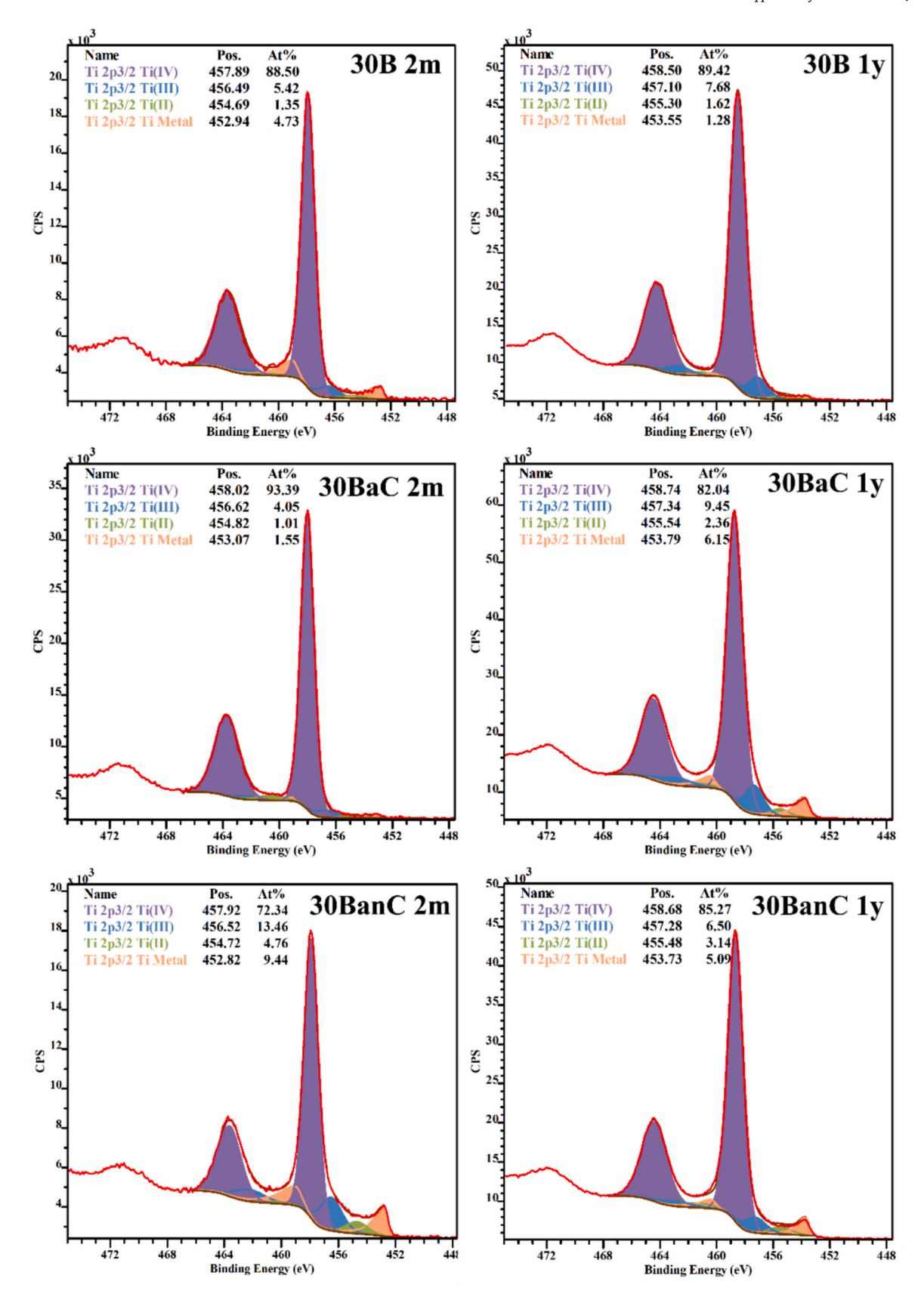


Fig. 3. XPS high-resolution scans for Ti 2p (475–447 eV) for each sample at two months (t = 2m) and 1 year (t = 1y) incubation at 30 °C. Deconvoluted to show different oxidation states.

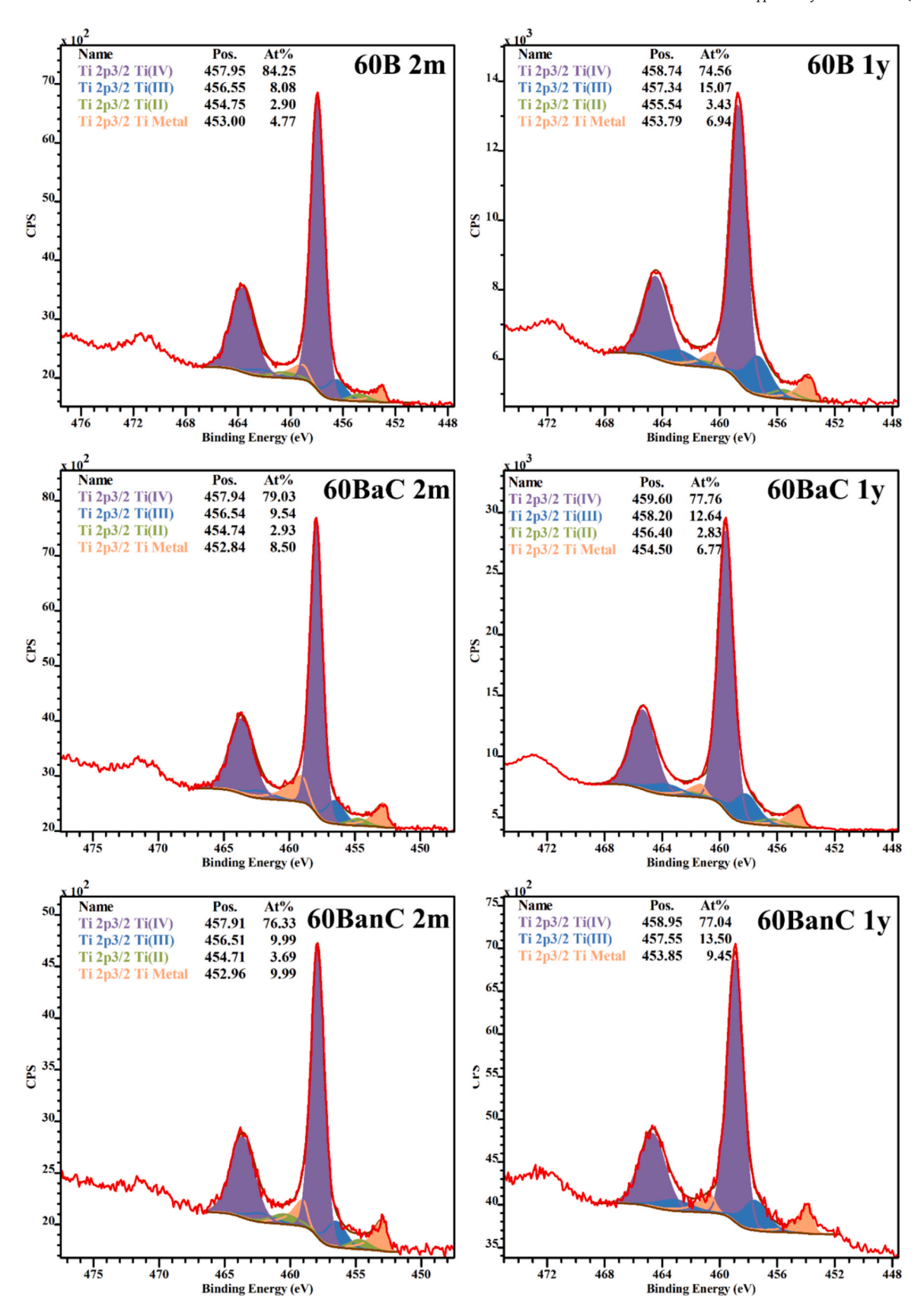


Fig. 4. XPS high-resolution scans in the Ti 2p (475–447 eV) region for each treatment at two months (t = 2m) and 1 year (t = 1y) incubation at 60 °C. Deconvoluted to demonstrate variation of oxidation states.

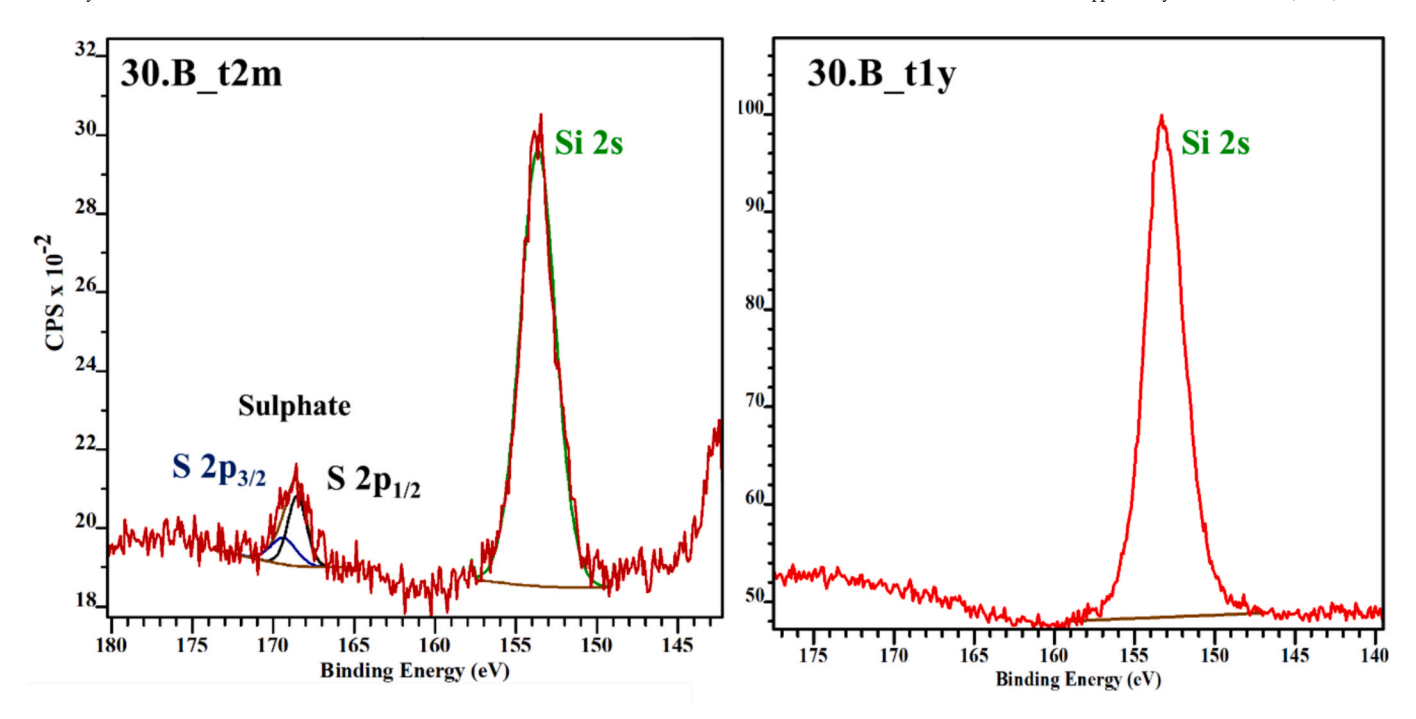


Fig. 5. High-resolution XPS spectra of the S 2p region (175-145 eV) on the surface of 30B after 2 months (left) and 1 year (right) exposure.

such as rutile, typically formed at 60 °C, enhance resistance to microbial sulphide attack and hydrogen embrittlement [66]. A higher proportion of  ${\rm TiO_2}$  on the surface suggests sufficient integrity of the passive layer, which is essential for maintaining titanium long-term corrosion resistance in SRB-influenced and anoxic environments [66,67].

Knowing this, high-resolution XPS spectra of S (Fig. 7) were acquired to check/monitor potential microbial sulphur caused damage on the titanium discs. The S 2p region (175–145 eV) was scanned to determine the speciation of sulphur and to distinguish between the added sulphates ( $SO_4^{2-}$ ) and the formation of sulphides ( $S^{2-}$ ). The presence of metal sulphides can be an indicator of MIC, due to the production of HS<sup>-</sup> by SRB, followed by its reaction with H<sup>+</sup> (Eqs. (2) and (3)).

$$SO_4^{2-} + 9H^+ + 8e^- \rightarrow HS^- + 4H_2O$$
 (2)

$$HS^- + H^+ \rightleftharpoons H_2S$$
 (3)

When  $TiO_2$  dominates on the surface of titanium metal, it is generally resistant to sulphide-induced corrosion. However, in sulphide rich environments, this passive layer can be disrupted by  $H_2S$  to form  $TiS_2$  (Eq. (4)), reducing the corrosion resistance of the material and potentially allowing  $S^{2-}$  to react with the titanium metal, producing far less protective TiS on the surface and degrading the material (Eq. (5)).

$$TiO_2 + 2H_2S \rightarrow TiS_2 + 2H_2O \tag{4}$$

$$Ti + H_2S \rightarrow TiS + H_2 \tag{5}$$

Fig. 5 shows an example spectrum of the S 2p region on the surface of sample 30B. A peak identified around 168 eV, commonly attributed to sulphates, showed S  $2p_{3/2}$  and S  $2p_{1/2}$  contributions at 169 and 168 eV respectively, after deconvolution [68,69]. To the right of this peak, another could be observed at around 155 eV, which can be assigned to Si 2 s, specifically from SiO\_2, a common component in bentonite [70]. No sulphide peaks attributed to TiS/TiS\_2 were detected on the scanned areas of the discs (See supplementary information S6), suggesting no evidence of MIC on the titanium disc surfaces. This outcome may be attributed to the integrity of the protective TiO\_2 layer remaining intact or not being sufficiently thinned to compromise its protective function. This is a promising result, demonstrating the potential resilience of

titanium under a 'worst-case' scenario simulated within the microcosms after the respective incubation times.

#### 3.3. Micro-FTIR

Micro-FTIR was used to analyse the surface of the titanium discs, allowing for the identification of key functional groups associated with microbial activity, such as proteins, lipids, and polysaccharides. This non-destructive technique provides detailed insights into bacterial interactions with surfaces by detecting and mapping organic compounds, characteristic of microbial cells and extracellular polymeric substances (EPS). As shown in Fig. 6, the discs were scanned using an integrated microscope to enable the comparison between spectra and visual artifacts.

The dark diffuse areas seen from the microscopic images in Fig. 6 correlate to residual bentonite remaining adhered to the disc surface. However, when the sample is irradiated with IR light, a false-colour image is obtained, displaying the presence and position of IR-absorbing molecules much clearer than in the optical images. On the left of each false-colour image lies an absorbance scale bar, which indicates the approximate level of absorbance correlating to the colour presented in each area. Higher absorbance values at any specific wavenumber range are directly related to a higher abundance of the corresponding functional group.

The false-colour images in Fig. 6 demonstrate the absorption of IR-bands intrinsic of amide I and II groups (1640 and 1540 cm<sup>-1</sup>). Amide group bands, associated with proteins, are inherently present in every FTIR spectrum of bacterial cells. The lack of these bands in the other scanned regions of the discs could indicate the absence of bacterial cells. Protein-related signals might also arise from molecules released during cell lysis or secreted extracellular polymeric substances (EPS).

Both 30B and 30BanC, in Fig. 8, showed evidence of amide I, II, and III on the surface after 2 months and 1 year of incubation. This observation was consistent on all scanned discs. Amide I arises primarily due to the C=O stretching vibrations in the peptide bond and occurs at around 1640 cm<sup>-1</sup> [71,72]. The amide II band is caused by the combination of C-N stretching and the in-plane N-H bending vibrations in the peptide bond, which normally appears around 1540 cm<sup>-1</sup> [71,72]. The

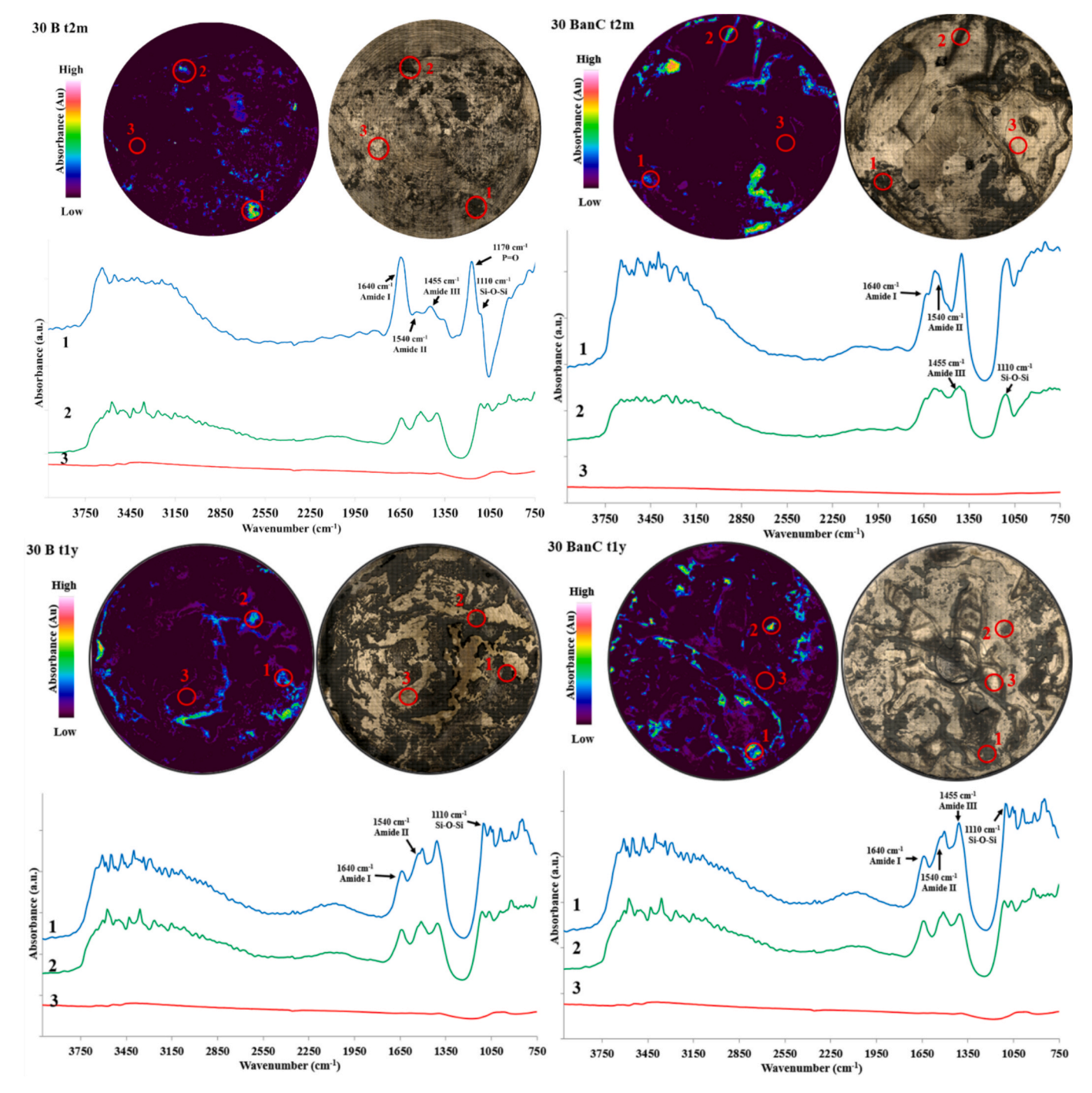


Fig. 6. Micro-FTIR analyses of samples incubated at 30 °C: 30B t = 2m (top left), 30BanC t = 2m (top right), 30B t = 1y (bottom left) and 30BanC t = 1y (bottom right). Figure depicts a microscope image of each of the discs surface with a chemical map showing the presence of amide I&II bands on the surface.

amide III band is mainly due to the C–N stretching,  $CH_2$  wagging, and N–H bending vibrations and are present at approximately 1440 cm<sup>-1</sup> [72]. Lastly, all samples also showed a peak commonly attributed to Si–O–Si stretching at around 1100 cm<sub>,</sub><sup>-1</sup> a common component of bentonite [73].

The detection of amide I, II, and III bands on the scanned discs provides strong evidence for the presence of bacteria or their byproducts, given their direct correlation to proteins. In the case of sample 30B (without bacterial consortia added), this result is mainly due to the indigenous bacteria present in the bentonite before and after incubation. In contrast, for sample 30BanC (anaerobic bacterial consortium added), the presence of the introduced bacteria, in both after 2 months

and 1 year of incubation under GDF relevant conditions, is confirmed. These signatures indicate that microbial material from the inoculated consortia remained detectable over the entire incubation period, consistent with their persistence in the bentonite matrix.

Although bacterial presence was detected on the scanned discs, XPS analysis revealed no evidence that these microorganisms altered the surface of the titanium disc after 2 months and 1 year of incubation. This may be explained by the possibility that the bacteria did not adhere directly to the metal surface but instead resided in/on the bentonite attached to the discs [22]. This is supported by the fact that spectra showing bands indicative of bacteria are always in conjunction with the presence of the Si-O-Si bands, related to the presence of bentonite clay.

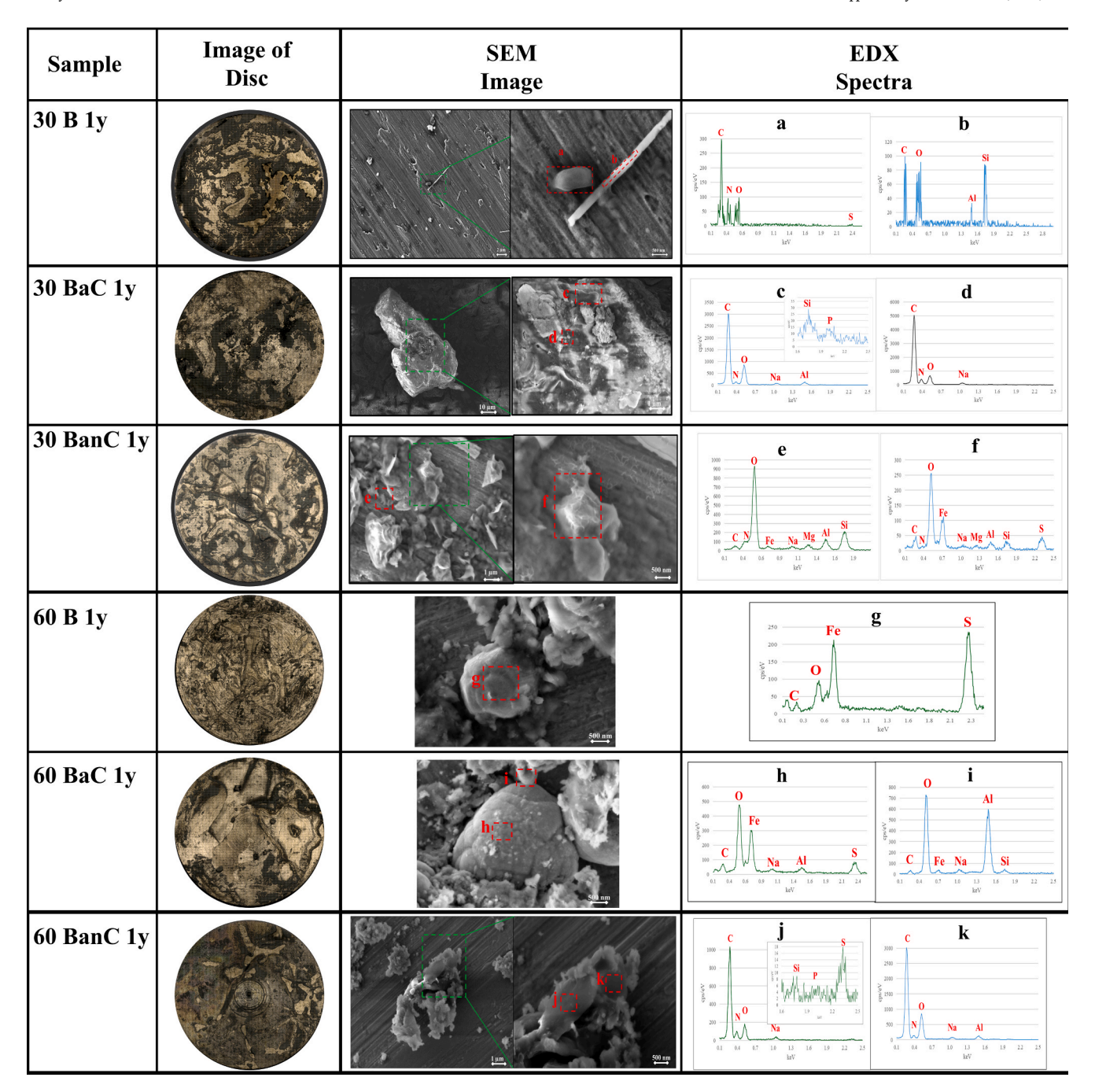


Fig. 7. SEM-EDX results for all samples incubated for 1-year. Includes images of the discs, SEM images of areas of interest and their corresponding EDX spectra.

Furthermore, when comparing the microscope images to the false-colour chemical absorption maps (Fig. 6), it becomes evident that regions exhibiting higher amide band absorption correlate with the dark bentonite deposits present on the disc surfaces. Alongside this, areas of the bare metal surface on the scanned discs did not demonstrate any evidence of proteins or any other IR absorbing compounds.

Samples of bentonite adhering to the discs were collected after 1 year of incubation and analysed using ATR-FTIR, mainly to investigate whether the bacterial signatures observed on the titanium disc surfaces originated from the adhered residual bentonite. The samples were dried at 40  $^{\circ}\text{C}$  for 72 h prior the analyses to mitigate the overlap of amide I band and water. This resulted in minimal change in intensity at 1640 cm $^{-1}$ , suggesting that the peak corresponds to amide I (Supplementary Information S7). The resulting spectra for all samples showed absorption bands at approximately 1640 cm $^{-1}$  and 1440 cm $^{-1}$ , corresponding to the

amide I and III regions respectively, alongside prominent Si-O-Si stretching bands at around  $1100~\rm cm^{-1}$ , characteristic of bentonite [71–73]. However, only samples from the microcosms incubated at 60 °C demonstrated bands corresponding to amide II at 1540 cm<sup>-1</sup>.

The detection of amide bands within the bentonite strongly suggests the presence of microbial cells and/or their extracellular products embedded within the matrix. These findings reinforce the observations made during the Micro-FTIR analyses of the titanium disc surfaces, where amide-related absorption was consistently co-located with bentonite deposits and was not seen directly on the exposed-titanium surface. This suggested that microbial colonisation in the microcosms was primarily confined to the bentonite, rather than involving direct adhesion to the titanium surface. As such, the lack of titanium surface alteration, detected by XPS after 2 months and 1 year of incubation, is likely a consequence of the bacteria not establishing direct contact with the metal substrate.

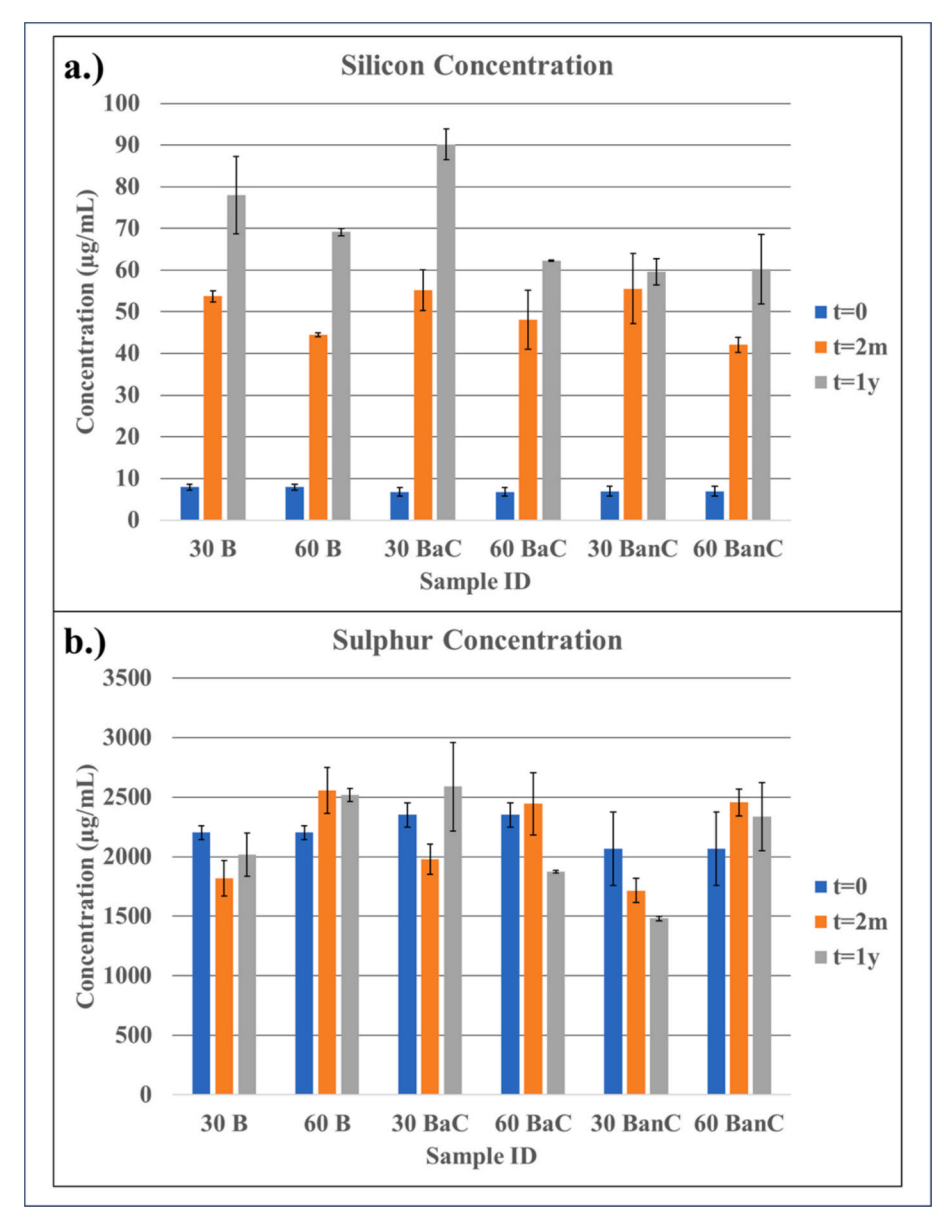


**Fig. 8.** (a.) Concentration of Silicon (Si-28) detected in the pore-water from the experimental microcosms including time zero (t = 0), 2 months (t = 2m), and 1-year (t = 1y) anoxic incubation. (b.) Concentration of Sulphur (S-34) detected in the sample pore-water from the experimental microcosms including time zero (t = 0), 2 months (t = 2m), and 1-year (t = 1y) anoxic incubation.

Taken together, the FTIR results show that microbial signals were consistently associated with bentonite deposits, reinforcing that titanium surfaces themselves remained free of detectable MIC.

#### 3.4. SEM-EDX

As part of the multimethod approach undertaken to complete this work, scanning electron microscopy coupled with energy-dispersive X-ray spectroscopy (SEM–EDX) was used to further investigate the surface of the titanium discs after incubation. SEM provided high-resolution imaging to assess morphological features, while EDX enabled semi-quantitative elemental analysis of adhered residues or potential corrosion products.

Bentonite deposits were found adhered to the surface of discs from all treatments. On samples incubated at 30 °C, visual and EDX-based evidence of bacterial presence was also observed. A cylindrical structure consistent with a bacterial cell morphology is observed in the SEM images of sample 30 B after 1 year of incubation, shown in Fig. 7. The

accompanying EDX spectra detected signals for carbon (C), predominantly from sample coating, along with nitrogen (N), and oxygen (O), both potentially suggestive of biological origin (spectrum a). Adjacent to this cell-like structure was a rod-shaped deposit, with EDX analysis identifying elements (Al and Si) typical of feldspar, a mineral commonly present in bentonite (spectrum b). The co-localisation of a bacterial cell with bentonite is evidence of the presence of indigenous bacteria, which have shown to be prone to preserve their cellular integrity. This could be an indication that they may potentially be, or become, metabolically active, however, SEM–EDX alone cannot resolve whether these structures reflect viable cells or preserved remnants of indigenous bentonite-associated microbes. These findings are consistent with reports highlighting the role of bentonite-resident microbial communities in producing extracellular polymeric substances (EPS) and interacting with mineral substrates under stress conditions [74].

Similar observations were made for discs from microcosms incubated at 30  $^{\circ}$ C with an aerobic bacterial consortium added (30 BaC). Deposits resembling bentonite were present, and SEM–EDX showed structures

suggestive of bacterial colonisation. Fig. 7 displays a region containing such a deposit, with EDX spectra from two distinct areas (spectra c and d). Both spectra revealed C, N, O, S, and P signals. The combination of these elements and the amorphous surface morphology is characteristic of EPS and other bacterial extracellular products [74]. These features could imply the presence of viable or metabolically active bacteria and support the interpretation of bacterial involvement in EPS formation [75].

Samples treated with the anaerobic consortium (30 BanC) showed comparable results. Fig. 7 displays SEM images of adhered bentonite at two magnifications, with two associated EDX scans. Spectrum e showed prominent C, N, and O signals alongside typical bentonite elements, again suggesting microbial EPS or biomass. Signals corresponding to iron (Fe) and sulphur (S) were observed in spectrum f. The close spatial proximity between the Fe and S compounds and C/N/O-rich material could support the hypothesis that microbial sulphate-reducing activity altered bentonite iron oxides, producing iron sulphide as a byproduct. The presence of SRB in this consortium, which generate hydrogen sulphide (HS<sup>-</sup>), further supports this analysis.

In contrast, titanium discs incubated at 60 °C exhibited markedly reduced evidence of bacterial activity. Sample 60 B displayed bentonite residues and EDX signals for Fe and S (Fig. 7, spectrum g). However, no microbial morphologies or EPS-like deposits were apparent. Similarly, in sample 60 BaC (Fig. 7, spectra h and i), Fe and S were detected, but no substantial indication of microbial presence were observed. These findings may imply that elevated temperatures reduced microbial viability or activity. It is also possible that iron sulphide formed through abiotic mechanisms, such as thermal transformation of iron-bearing bentonite components, rather than biological [76].

On the other hand, evidence of microbial activity was detected in a sample incubated at 60  $^{\circ}$ C (after 1 year) with added anaerobic bacteria (60 BanC). Fig. 7 shows a bentonite structure adhered to the surface, alongside EDX spectra indicating the presence of C, N, O, and S in conjunction with Al and Si—elements typical of bentonite (spectra j and k). The high counts of carbon, as well as the size and shape of the structure, could suggest that bacterial components or debris are present.

Aside from the presence of bentonite-related deposits, the titanium surfaces remained smooth and featureless, consistent with the preservation of the passive TiO<sub>2</sub> layer. No visible pitting, roughening, or formation of titanium–sulphur compounds was observed. These results indicated that, although microbial activity may have occurred in some cases, there was no apparent effect on the titanium surface itself.

Overall, the SEM-EDX observations are consistent with data obtained from XPS and micro-FTIR analyses, confirming that titanium maintained a stable, protective oxide layer throughout the biotically stimulated one-year incubation period. While microbial structures and metabolic by-products were observed in co-localisation with bentonite, direct colonisation or degradation of the titanium surface was minimal. These findings reinforce the potential suitability of titanium as a corrosion-resistant material for the long-term containment of high-level radioactive waste under simulated GDF conditions, even in the presence of microbial activity. Collectively, these observations emphasise that microbial signals were consistently associated with bentonite deposits rather than the titanium surface, supporting the interpretation that any biotic processes occurred in the clay matrix without compromising titanium's integrity.

#### 3.5. ICP-MS

Additional to the microscopic and spectroscopic techniques, ICP-MS was employed to further investigate the chemical evolution of the porewater during incubation period, and quantify the concentrations of key elements, such as Ti, Al, Si, and S. Only silicon and sulphur exhibited clear trends over time. Dissolved silicon (see Fig. 8a) increased from below 10  $\mu$ g/mL at time zero, to >50  $\mu$ g/mL by one year in all treatments, consistent with gradual dissolution of the bentonite silicate minerals. In contrast, dissolved aluminium, and iron remained at trace

levels (<0.1 and <0.8  $\mu g/mL$ , respectively, see supplementary information S8).

As previously mentioned, the most severe case of blackening of the pore-water occurred in the 30 °C microcosms, which coincided with the largest drop in aqueous sulphur (Fig. 8b). In the 30 °C treatments with either the native bentonite microbiota (30 B) or the added anaerobic consortium (30 BanC), sulphur (added initially as sulphate) concentrations decreased over the 1-year incubation period by 497 and 1176 ug/ mL, respectively. In contrast, sample 30 BaC did not see a substantial change in sulphur concentrations. For samples incubated at 60 °C, only the microcosms that contained addition bacterial consortia (60 BaC and 60 BanC) exhibited a decrease in sulphur concentration, with values of 930 and 148  $\mu$ g/mL, respectively. The decrease in concentration for both 60 and 30 °C samples could all be attributed to microbial activity as SRB in bentonite systems are known to consume sulphate under anoxic conditions [10]. The hydrogen sulphide produced could react with Fe<sup>2+</sup> ions to precipitate iron-sulphide phases (such as FeS or Fe<sub>3</sub>S<sub>4</sub>) that are dark in colour [77]. In line with this mechanism, the 30 °C microcosms showed intense darkening as sulphur was depleted, whereas the 60 °C experiments showed only mild colour changes, except for the sample 60 BaC, with additional aerobic consortia. These observations are consistent with previous studies where H<sub>2</sub>S-induced FeS formation leads to visible blackening of bentonite materials [33,42,77]. Notably, iron concentrations in solution remained at sub-ppm levels throughout, confirming that it is the formation of insoluble sulphides, not dissolved iron, that accounts for the darkening. This provides a geochemical explanation for the visual blackening trends observed in the microcosms and links the pore-water chemistry directly to the colour changes described in Section 3.1.

Dissolved titanium remained below detection limits in almost all samples. No anomalous titanium release was detected in the SRB-active (30  $^{\circ}\text{C}$ ) microcosms, despite potential sulphide generation. Although sulphide species can, under extreme conditions, compromise titanium's passive oxide layer and initiate corrosion [25]. However, in this study no such effects were observed. The lack of detectable Ti release, even in the most sulphide-rich microcosms, underscores the robustness of the passive TiO2 layer under biotically influenced conditions. The titanium discs maintained their surface integrity, consistent with the high stability of TiO2 under anoxic conditions. Overall, the ICP-MS results support the interpretation that while microbial sulphate reduction and FeS precipitation could have occurred, the titanium discs themselves remained resistant to both biotic and abiotic corrosion under the simulated GDF conditions.

#### 4. Conclusion

As titanium being considered one of the candidate canister materials for the long-term storage of nuclear waste in future Geological Disposal Facilities (GDFs), a detailed investigation into the corrosion behaviour of this material was conducted. This study assessed the resistance of titanium to MIC under biotically stimulated, sulphur-rich, anaerobic conditions, representing a *worst-case* biogeochemical scenario relevant to geological disposal.

XPS analysis of the titanium discs exposed to anoxic conditions for up to 1 year at 30 °C and 60 °C in pore-water saturated bentonite, with and without added bacterial consortia, consistently demonstrated minimal thinning of  $\rm TiO_2$  passive layer on the sample surfaces. Coupling this with SEM-EDX, surface analyses showed no significant degradation, pitting, or sulphide-induced corrosion on the titanium. Furthermore, micro-FTIR revealed evidence of amide I, II, and III bands on the surface of the discs, indicating that microbial presence was always co-located with bentonite. Microbial colonisation was suggested to be only confined to the nearby bentonite residues adhered to the titanium surfaces, with no direct biofilm formation or corrosion features observed on the actual metal surfaces. This cross-validation between XPS, SEM–EDX, FTIR, and ICP-MS strengthens the interpretation that microbial processes remained

confined to bentonite and did not compromise titanium surfaces.

These findings demonstrate titanium's exceptional stability against anaerobic biocorrosion, even in environments rich in microorganisms. The results support the suitability and structural viability of titanium as a candidate material for HLW canisters, particularly when used in combination with bentonite buffers. In practical terms, this suggests that even under conditions deliberately designed to accelerate microbial activity and sulphide generation, titanium retains its protective oxide layer and resists microbiologically influenced corrosion. Furthermore, this study highlights the importance of explicitly considering microbial influences in repository safety assessments, even for corrosion-resistant materials.

Although highly encouraging, longer-term studies, investigation of titanium alloys, and evaluation under evolving bentonite geochemistry are warranted to confirm titanium performance over repository timescales. Nevertheless, the data presented here provides strong evidence that titanium can maintain its protective properties under realistic and challenging repository-relevant conditions, contributing to the long-term safety of geological disposal concepts.

Future work should include detailed characterisation of the bacterial communities within the microcosms to better understand their metabolic activity, resilience, and any shifts over time. Analysing these communities would provide valuable insights into microbial function and clarify whether the presence of titanium influences community composition or behaviour. This could reveal important interactions between candidate materials and bentonite-resident microbes under repository-relevant conditions. Further investigation of the microbial populations already present in these microcosms would enhance future understanding and provide a foundation for subsequent studies. Additionally, in-situ, longterm testing of candidate materials under biotically stimulated, GDFrelevant environments is recommended to validate laboratory findings and evaluate material performance over repository timescales. Together, these approaches would support a more comprehensive understanding of microbe-material interactions and contribute to the robust safety assessment of geological disposal systems.

#### CRediT authorship contribution statement

Adam D. Mumford: Writing – original draft, Project administration, Methodology, Investigation, Formal analysis, Data curation, Conceptualization. Marcos F. Martinez-Moreno: Writing - review & editing, Methodology, Investigation, Conceptualization. Mar Morales-Hidalgo: Writing - review & editing, Methodology, Investigation, Conceptualization. Cristina Povedano-Priego: Writing - review & editing, Methodology, Investigation, Conceptualization. Lidia Generelo-Casajus: Writing - review & editing, Methodology, Investigation. Fadwa Jroundi: Writing - review & editing, Supervision. Lorna Anguilano: Writing - review & editing, Resources, Data curation. Uchechukwu Onwukwe: Writing - review & editing, Resources, Data curation. Philip H.E. Gardiner: Writing - review & editing, Resources, Conceptualization. Mohamed L. Merroun: Writing - review & editing, Supervision, Resources, Methodology, Funding acquisition, Conceptualization. Yon Ju-Nam: Writing - review & editing, Supervision, Methodology, Funding acquisition, Conceptualization. Jesus J. Ojeda: Writing - review & editing, Supervision, Project administration, Methodology, Funding acquisition, Conceptualization.

#### 5. Funding

MLM acknowledges funds from grant PID2022\u2013138402NB-C21 funded by MICIU/AEI/10.13039/501100011033 and by ERDF. In addition, this work was funded by EURAD 1 & 2 initiatives under H2020-EURATOM (grant agreements 847593 and 101166718) awarded to MLM. MMH acknowledges support from grant FPU20/00583 from the Spanish Ministry of Universities. ADM acknowledges funding from the UK Engineering and Physical Sciences Research Council (EPSRC) DTP scholarship (project reference: 2748843).

#### **Declaration of competing interest**

The authors declare that they have no known competing financial interests or personal relationships that could have appeared to influence the work reported in this paper.

#### Acknowledgements

The authors would like to thank Dr Ashley Howkins from the Experimental Techniques Centre (ETC) at Brunel University, London, for his help during the SEM-EDX analysis. Also, thanks to Dr. James McGettrick from the School of Engineering and Applied Sciences at Swansea University, for supporting XPS data acquisition. Lastly, a big thanks to Michael Cox and Shania Laming from the Analytical Laboratory in Sheffield Hallam University for their help with ICP-MS data acquisition.

#### Appendix A. Supplementary data

Supplementary data to this article can be found online at https://doi.org/10.1016/j.apsusc.2025.164779.

#### Data availability

Data will be made available on request.

#### References

- [1] M. Lehtonen, The governance ecosystem of radioactive waste management in france: governing of and with mistrust, in: M. Arentsen, R. van Est (Eds.), The Future of Radioactive Waste Governance: Lessons from Europe, Springer Fachmedien Wiesbaden, Wiesbaden, 2023, pp. 231–257.
- [2] Y.-M. Lee, C.-H. Kang, Y.-S. Hwang, Nuclide release from an HLW repository: development of a compartment model, Ann. Nucl. Energy 34 (10) (2007) 782–791.
- [3] E. Weetjens, Update of the near field temperature evolution calculations for disposal of UNE-55, MOX-50 and vitrified HLW in a supercontainer- based geological repository, 2009
- [4] IAEA, Status and Trends in Spent Fuel and Radioactive Waste Management. 2022, International Atomic Energy Agency, Vienna.
- [5] IAEA, International Atomic Energy Association (IAEA) Safety Standards for nuclear waste disposal.pdf>. 2012.
- [6] B. Little, P. Wagner, An overview of microbiologically influenced corrosion of metals and alloys used in the storage of nuclear wastes, Can. J. Microbiol. (1996).
- [7] A.R. Brown, C. Boothman, S.M. Pimblott, J.R. Lloyd, The impact of gamma radiation on sediment microbial processes, Appl. Eviron. Microbiol. 81 (2015).
- [8] R. Zuo, et al., Inhibiting mild steel corrosion from sulfate-reducing bacteria using antimicrobial-producing biofilms in Three-Mile-Island process water, Appl. Microbiol. Biotechnol. 64 (2) (2004) 275–283.
- [9] P.C. Petit, O. Pible, V.V. Eesbeeck, C. Alban, G. Steinmetz, M. Mysara, P. Monsieurs, J. Armengaud, C. Rivasseau, Direct meta-analyses reveal unexpected microbial life in the highly radioactive water of an operating nuclear reactor core, Microorganisms 8 (12) (2020) 1857.
- [10] M.A. Ruiz-Fresneda, M.F. Martinez-Moreno, C. Povedano-Priego, M. Morales-Hidalgo, F. Jroundi, M.L. Merroun, Impact of microbial processes on the safety of deep geological repositories for radioactive waste, Front. Microbiol. 14 (2023).
- [11] M. Lopez-Fernandez, C.A.R. Vilchez-Vargas, I. Sanchez-Castro, M.L. Merroun, Bacterial Diversity in Bentonites, Engineered Barrier for Deep Geological Disposal of Radioactive Wastes, Microb. Ecol. 70 (2015).
- [12] M. Lopez-Fernandez, O. Fernández-Sanfrancisco, A. Moreno-Garcia, I. Martinez-Sanchez, I. Sanchez-Castro, M.L. Merroun, Microbial communities in bentonite formations and their interactions with uranium, Appl. Geochem. 49 (2014).
- [13] M. Lopez-Fernandez, R. Vilchez-Vargas, F. Jroundi, N. Boon, D. Pieper, M. L. Merroun, Microbial community changes induced by uranyl nitrate in bentonite clay microcosms, Appl. Clay Sci. 160 (2018) 206–216.
- [14] C. Povedano-Priego, J.F.M. Lopez-Fernandez, R. Strestha, R. Spanek, I. Martinez-Sanchez, M.V.V. Villar, A. Sevcu, M. Dopson, M.L. Merroun, Deciphering indigenous bacteria in compacted bentonite through a novel and efficient DNA extraction method: Insights into biogeochemical processes within the Deep Geological Disposal of nuclear waste concept, J. Hazard. Mater. 408 (2021).
- [15] S. Chen, P. Wang, D. Zhang, Corrosion behavior of copper under biofilm of sulfatereducing bacteria, Corros. Sci. 87 (2014) 407–415.
- [16] M.F. Martinez-Moreno, C. Povedano-Priego, M. Morales-Hidalgo, A.D. Mumford, J. J. Ojeda, F. Jroundi, M.L. Merroun, Impact of compacted bentonite microbial community on the clay mineralogy and copper canister corrosion: a multidisciplinary approach in view of a safe Deep Geological Repository of nuclear wastes, J. Hazard. Mater. (2023).

- [17] C. Povedano-Priego, et al., Indigenous bacterial adaptation and survival: Exploring the shifts in highly compacted bentonite over a 5-year long-term study for nuclear repository purposes, J. Hazard. Mater. 489 (2025) 137526.
- [18] J.-S. Kim, et al., Geological storage of high level nuclear waste, KSCE J. Civ. Eng. (2011).
- [19] A. Abdelouas, A.U., R. Bernier-Latmani C. Bosch A. Cherkouk D. Dobrev A.M. Fernández N. Finck Gaggiano R.,, H.J. Havlová V., Idiart A., Mijnendonckx K., Montoya V., Muñoz A.G., Padovani, C., Pont A., Rajala P., Riba O., Sarrasin, S.S. L., Smart N., Texier-Mandoki N., Wersin P., Initial State-of-the-Art of WP ConCorD, 2022
- [20] N. Diomidis, L.H. Johnson, Materials options and corrosion-related considerations in the design of spent fuel and high-level waste disposal canisters for a deep geological repository in opalinus clay, JOM 66 (3) (2014) 461–470.
- [21] Q. Zhang, et al., On the long term estimation of hydrogen embrittlement risks of titanium for the fabrication of nuclear waste container in bentonite buffer of nuclear waste repository, J. Nucl. Mater. 533 (2020) 152092.
- [22] D.S. Hall, et al., An evaluation of corrosion processes affecting copper-coated nuclear waste containers in a deep geological repository, Prog. Mater Sci. 118 (2021)
- [23] F. King, Durability of High Level Waste and Spent Fuel Disposal Containers-an overview of the combined effect of chemical and mechanical degradation mechanisms Appendix B. 5-Corrosion of Titanium Alloys, 2014.
- [24] F. King, Container materials for the storage and disposal of nuclear waste, Corros. Sci. (2013).
- [25] D.W. Shoesmith, B.M. Ikeda, The resistance of titanium to pitting, microbially induced corrosion and corrosion in unsaturated conditions (No. AECL-11709). Atomic Energy Canada Limited, Pinawa, Manitoba (Canada); 1997.
- [26] M. Guo, The Electrochemical and Corrosion Study of copper for Nuclear Waste Containers under Deep Geological Disposal Conditions, The University of Western Ontario (Canada), Canada – Ontario, CA, 2020, 265.
- [27] C. Povedano-Priego, et al., Unlocking the bentonite microbial diversity and its implications in selenium bioreduction and biotransformation: advances in deep geological repositories, J. Hazard. Mater. 445 (2023) 130557.
- [28] A.M. Fernández, J. Cuevas, P. Rivas, Pore water chemistry of the febex bentonite, MRS Proc. 663 (2000) 573.
- [29] A.M. Fernandez, Pore-water composition for FEBEX Bentonite, M. Morales-Hidalgo (Ed.), 2023.
- [30] M. Morales-Hidalgo, et al., Long-term tracking of the microbiology of uranium-amended water-saturated bentonite microcosms: a mechanistic characterization of U speciation, J. Hazard. Mater. 476 (2024) 135044.
- [31] M. Lopez-Fernandez, et al., Effect of U(VI) aqueous speciation on the binding of uranium by the cell surface of Rhodotorula mucilaginosa, a natural yeast isolate from bentonites, Chemosphere 199 (2018) 351–360.
- [32] C. Povedano-Priego, et al., Shifts in bentonite bacterial community and mineralogy in response to uranium and glycerol-2-phosphate exposure, Sci. Total Environ. 692 (2019) 219–232.
- [33] C. Povedano-Priego, et al., Deciphering indigenous bacteria in compacted bentonite through a novel and efficient DNA extraction method: Insights into biogeochemical processes within the Deep Geological Disposal of nuclear waste concept, J. Hazard. Mater. 408 (2021) 124600.
- [34] M.A. Javed, W.C. Neil, G. McAdam, S.A. Wade, Effect of sulphate-reducing bacteria on the microbiologically influenced corrosion of ten different metals using constant test conditions, Int. Biodeter. Biodegr. 125 (2017).
- [35] N. Kip, J.A. van Veen, The dual role of microbes in corrosion, ISME J. 9 (3) (2015) 542–551.
- [36] D. Enning, J. Garrelfs, Corrosion of iron by sulfate-reducing bacteria: new views of an old problem, Appl. Environ. Microbiol. 80 (4) (2014) 1226–1236.
- [37] M. Morales-Hidalgo, et al., Gamma radiation in highly compacted FEBEX bentonite: key microbial and mineralogical behavior for safety assessment of nuclear repositories, J. Hazard. Mater. 495 (2025) 138915.
- [38] IAEA, Scientific and Technical Basis for the Geological Disposal of Radioactive Wastes. 2003, Vienna: International Atomic Energy Agency.
- [39] Nagra, Project Opalinus Clay: Safety Report Demonstration of disposal feasibility for spent fuel, vitrified high-level waste and long-lived intermediate-level waste (Entsorgungsnachweis), in Nagra Technical Report NTB 02-05, 2002.
- [40] Swedish Nuclear Fuel and Waste Management Co, Long-term safety for the final repository for spent nuclear fuel at Forsmark. Main report of the SR-Site project, SKB, Editor. 2011.
- [41] F. King, D.S. Hall, P.G. Keech, Nature of the near-field environment in a deep geological repository and the implications for the corrosion behaviour of the container, Corros. Eng. Sci. Technol. 52 (sup1) (2017) 25–30.
- [42] M.F. Martinez-Moreno, et al., Microbial influence in spanish bentonite slurry microcosms: Unveiling a-year long geochemical evolution and early-stage copper corrosion related to nuclear waste repositories, Environ. Pollut. 358 (2024) 124491.
- [43] M.F. Martinez-Moreno, et al., Microbial responses to elevated temperature: evaluating bentonite mineralogy and copper canister corrosion within the longterm stability of deep geological repositories of nuclear waste, Sci. Total Environ. 915 (2024) 170149.
- [44] M.F. Martinez-Moreno, et al., Dual effect of Se(IV) and bentonite microbial community interactions on the corrosion of copper and Se speciation: Implication on repository safety assessment, Sci. Total Environ. 965 (2025) 178613.
- [45] N. Fairley, et al., Systematic and collaborative approach to problem solving using X-ray photoelectron spectroscopy, Appl. Surf. Sci. Adv. 5 (2021) 100112.

- [46] N. Matschiavelli, et al., The year-long development of microorganisms in uncompacted bavarian bentonite slurries at 30 and 60 °C, Environ. Sci. Technol. 53 (17) (2019) 10514–10524.
- [47] H. Miettinen, et al., Transformation of inherent microorganisms in Wyoming-type bentonite and their effects on structural iron, Appl. Clay Sci. 221 (2022) 106465.
- [48] K. Pedersen, et al., Mobility and reactivity of sulphide in bentonite clays Implications for engineered bentonite barriers in geological repositories for radioactive wastes, Appl. Clay Sci. 146 (2017).
- [49] C. Rolland, et al., Microbial hydrogen sinks in the sand-bentonite backfill material for the deep geological disposal of radioactive waste, Front. Microbiol. 15 (2024).
- [50] C. Mota-Heredia, J. Cuevas, R. Fernández, Effect of iron chloride (II) on bentonites under hydrothermal gradients: a comparative study between sodium bentonite and calcium bentonite, Minerals 14 (2024), https://doi.org/10.3390/min14020132.
- [51] D. Rickard, G.W. Luther, Chemistry of iron sulfides, Chem. Rev. 107 (2) (2007) 514–562.
- [52] Y. Wang, S. Kern, D. Newman, Endogenous phenazine antibiotics promote anaerobic survival of pseudomonas aeruginosa via extracellular electron transfer, J. Bacteriol. 192 (2010) 365–369.
- [53] H. Shiratori, et al., Clostridium clariflavum sp. nov. and Clostridium caenicola sp. nov., moderately thermophilic, cellulose-/cellobiose-digesting bacteria isolated from methanogenic sludge, Int. J. Syst. Evol. Microbiol. 59 (7) (2009) 1764–1770.
- [54] L.L. Campbell, A. Frank Hilmer, R. Hall Elizabeth, Studies on thermophilic sulfate reducing bacteria I. Sporovibrio desulfuricansasClostridium nigrificans, J. Bacteriol. 73 (4) (1957) 516–521.
- [55] D.Y. Sorokin, et al., Anaerobic oxidation of thiosulfate to tetrathionate by obligately heterotrophic bacteria, belonging to the Pseudomonas stutzeri group, FEMS Microbiol. Ecol. 30 (2) (1999) 113–123.
- [56] Y. He, et al., Diversity of mixotrophic neutrophilic thiosulfate- and iron-oxidizing bacteria from deep-sea hydrothermal vents, Microorganisms 11 (2022) 100.
- [57] M. Biesinger, et al., Quantitative chemical state XPS analysis of first row transition metals, oxides and hydroxides, J. Phys. Conf. Ser. 100 (2008) 012025.
- [58] M.C. Biesinger, et al., Resolving surface chemical states in XPS analysis of first row transition metals, oxides and hydroxides: Sc, Ti, V, Cu and Zn, Appl. Surf. Sci. 257 (3) (2010) 887–898.
- [59] D. Gonbeau, et al., XPS study of thin films of titanium oxysulfides, Surf. Sci. 254 (1) (1991) 81–89.
- [60] A. Lebugle, et al., Experimental L and M Core Level Binding Energies for the Metals 22Ti to 30Zn, Phys. Scr. 23 (5A) (1981) 825.
- [61] Wagner, C.D., W.M. Riggs, L.E. Davis, J.F. Moulder, and G.E. Muilenberg Handbook of x- ray photoelectron spectroscopy. Perkin-Elmer Corporation, Phys. Electronics Div., Eden Prairie, Minnesota, USA. 1979.
- [62] S.-C. Kim, et al., Band structures of passive films on titanium in simulated bioliquids determined by photoelectrochemical response: principle governing the biocompatibility, Science and Technology of Advanced Materials 23 (1) (2022) 322–331.
- [63] J. Yang, et al., Research progress on the corrosion behavior of titanium alloys, Corros, Rev. 41 (2022).
- [64] J.J. Noel, The electrochemistry of titanium corrosion, PhD thesis, Department of Chemistry, University of Manitoba, Winnipeg, MB, Canada. 1999.
- [65] A. Seeber, et al., Sintering unalloyed titanium in DC electrical abnormal glow discharge, Mater. Res.-Ibero-Am. J. Mater. – Mater. Res.-Ibero-Am. J. Mater. 13 (2010).
- [66] C. Briant, The Electrochemistry, Corrosion and Hydrogen Embrittlement of Titanium, 2004, pp. 55–85.
- [67] D.E.J. Talbot, J.D.R. Talbot, Corrosion Science and Technology, third ed., Taylor & Francis, 2018.
- [68] B.R. Strohmeier, et al., Surface spectroscopic characterization of CuAl2O3 catalysts, J. Catal. 94 (2) (1985) 514–530.
- [69] H. Peisert, et al., Relaxation energies in XPS and XAES of solid sulfur compounds, J. Electron Spectrosc. Relat. Phenom. 68 (1994) 321–328.
- [70] T. Gross, et al., An XPS analysis of different SiO2 modifications employing a C 1s as well as an Au 4f7/2 static charge reference, Surf. Interface Anal. 18 (1) (1992) 59–64
- [71] J. Ojeda, et al., Characterization of the cell surface and cell wall chemistry of drinking water bacteria by combining XPS, FTIR spectroscopy, modeling, and potentiometric titrations, Langmuir 24 (2008) 4032–4040.
- [72] J. Ojeda, M. Romero-Gonzalez, S. Banwart, Analysis of bacteria on steel surfaces using reflectance micro-Fourier transform infrared spectroscopy, Anal. Chem. 81 (2009) 6467–6473.
- [73] D. Widjonarko, et al., Phosphonate modified silica for adsorption of Co(II), Ni(II), Cu(II), and Zn(II), Indon. J. Chem. 14 (2014) 143–151.
- [74] A. Rizvi, M. Saghir Khan, Putative role of bacterial biosorbent in metal sequestration revealed by SEM–EDX and FTIR, Indian J. Microbiol. 59 (2) (2019) 246–249.
- [75] G. Haddad, et al., A preliminary investigation into bacterial viability using scanning electron microscopy–energy-dispersive X-ray analysis: the case of antibiotics, Front. Microbiol. 13 (2022).
- [76] S. Kaufhold, et al., Chemical and mineralogical reactions of bentonites in geotechnical barriers at elevated temperatures: review of experimental evidence and modelling progress, Clay Miner. 58 (3) (2023) 280–300.
- [77] H. Estay, L. Barros, E. Troncoso, Metal sulfide precipitation: recent breakthroughs and future outlooks, Minerals 11 (2021), https://doi.org/10.3390/min11121385.